Rational design of melamine-crosslinked poly(ethylene glycol) membranes for sour gas purification

Dana A. Wong, Elizabeth E. Haddad, Sibo Lin, Seth A. Sharber, John Yang, John A. Lawrence III, Daniel J. Harrigan, Patrick T. Wright, Yang Liu, and Benjamin J. Sundell

Aramco Americas - Boston Research Center, Cambridge, MA 02139, USA

Keywords: Natural gas separations, Membrane, Acid Gas Enrichment, Melamine, PEG

Abstract

Natural gas accounts for 22% of the world's energy consumption [1]; however, most of the current natural gas reservoirs are sour. Sour natural gas containing significant amounts of hydrogen sulfide (H_2S) along with carbon dioxide (CO_2) must be purified to meet the strict requirements for transportation and storage in the industry. Sour natural gas purification involves two steps: acid gas removal (AGR) and acid gas enrichment (AGE), which both are expensive using current highly energy intensive technologies. Membrane separation represents the most attractive technology to lower the purification cost and the carbon footprint in these large applications. Guided by density functional theory (DFT) calculations, we rationally designed a crosslinked poly(ethylene glycol) (PEG) membrane for AGR and AGE applications. Specifically, PEG-bisazide monomers were crosslinked with a novel trialkyne-functionalized H_2S-philic melamine via azide-alkyne cycloaddition click chemistry. The developed membranes were characterized and tested for (H_2S+CO_2)/CH_4 and H_2S/CO_2 separations under realistic industrial conditions, targeting the AGR and AGE applications, respectively. These novel membranes achieved high H_2S permeability while maintaining attractive H_2S/CO_2 selectivity.

Introduction

Natural gas is expected to play a key role in the global energy shift toward renewables due to its high energy efficiency and low pollutants when compared to other fossil fuels such as coal or oil. The main component of natural gas is methane (CH_4), and when combusted this fossil fuel produces 30% and 43% fewer carbon dioxide (CO_2) emissions than oil and coal [2]. The U.S. Energy Information Administration (EIA) projected national natural gas production to increase to 42.1 trillion cubic feet by the year 2050 [3]. Sour gas reservoirs primarily contain methane but are contaminated with high levels of hydrogen sulfide (H_2S) and CO_2 along with other impurities (water, nitrogen, helium, heavy hydrocarbons etc.) [4]. One challenge hindering increased natural gas usage is that the number of untapped sweet natural gas reservoirs (containing < 4 ppm H_2S) is depleting, leaving the world to rely on sour natural gas reservoirs. It is estimated that approximately 40% of the natural gas reservoirs worldwide have large amounts of sour gas [5]. High levels of H_2S and CO_2 are problematic since H_2S is extremely toxic to humans, and both gases can cause corrosion to pipelines. To meet pipeline specifications natural gas streams must contain <2% CO_2 and <4 ppm H_2S.

The natural gas purification process is complex due to the large variety of impurities that are present, especially in the case of sour gas feeds. Fig. S1 depicts a process flow diagram of the different steps needed for the purification of raw natural gas. In the case of H_2S and CO_2 removal, there are two key separation processes where membranes have the potential to significantly reduce energy costs. The first separation process is known as acid gas removal (AGR), where H_2S and CO_2 are simultaneously removed from the stream. Conventional methods for this separation are carried out using cryogenic distillation, amine absorption, distillation, crystallization, or adsorption. However, more research is focused on replacing these technologies with membrane separation units since they are much more efficient in terms of energy requirements and cost [2]. Membranes for AGR are more suitable at high feed pressures due to the pressure-driven nature of this separation. Thus, developing membranes for this application is quite challenging since ideal separation conditions for AGR would occur under aggressive conditions and high pressures (> 55 bar) [2, 6, 7].

The second separation process dealing with acid gases, is known as acid gas enrichment (AGE), which separates H_2S (< 20 mol%) from CO_2 at lower pressures (~14 bar) [6, 7]. To reduce the hazards associated with H_2S gas waste, it will typically be sent to a sulfur recovery unit (SRU), such as a Claus reactor, where H_2S is converted into elemental sulfur. For efficient conversion to sulfur in the Claus unit, H_2S must be present in high concentrations (> 55 mol%) in the feed for a couple of reasons. The first is that high H_2S concentration increases the temperature in the furnace. A key requirement of the Claus reactor is to maintain high temperatures around 1700 ^oC to maintain a stable flame in the reactor. If a H_2S stream contains high amounts of CO_2, it reduces the furnace temperature, thus increasing energy requirements to operate the reactor [6]. Additionally, it is essential to reduce the CO_2 concentration to eliminate the possibility of unfavorable reactions between CO_2 and H_2S. When these acid gases react, they can form carbonyl sulfide (COS) and carbon disulfide (CS_2) in the SRU, which later convert into environmentally harmful sulfur dioxide (SO_2) [8]. As a result of these requirements, AGE is necessary to concentrate the H_2S stream and separate it from the CO_2 gas prior to the sulfur recovery step. The state-of-the-art technology for acid gas enrichment involves using amine absorption solvents such as methyldiethanolamine (MDEA) or other sterically hindered amines [9]. This current technology is energy-intensive and costly due to the need for thermal regeneration [10]. Utilizing membranes for AGE has not been widely explored but would drastically improve the energy and cost requirements.

Poly(ethylene glycol) (PEG) containing materials have been of high interest for rubbery polymers for membrane gas separations, exhibiting high CO_2 solubility, permeability, and selectivity (CO_2/N_2 or CO_2/CH_4) [11-13]. The polar ether groups from the PEG chain have good CO_2 affinity due to the Lewis acid-base interactions, resulting in enhanced CO_2 permeability and selectivity. Numerous studies have found that crosslinkers can enhance PEG membrane gas separations [14-16], as crosslinkers can disrupt crystallinity (increasing gas permeation) while enhancing mechanical strength and resistance to detrimental plasticization effects. Previous work in our lab explored crosslinking PEG membranes with a methylidynetri-*p*-phenylene triisocyanate (PTI) crosslinker, but found the top-performing member of this family of membranes to be brittle and have decreased CO_2 permeability (< 100 Barrer) [14]. To improve upon the PEG-PTI membranes

for AGE (H_2S/CO_2 separation), we sought to incorporate amine-based crosslinkers. While amines are well-known to facilitate transport of CO_2 through membranes [13, 17, 18], amine solvents are also the conventional technology for AGE, and amine-functionalized solid sorbents are able to capture H_2S [19]. Peng *et al*. demonstrated that amine-functionalization improves H_2S/CO_2 selectivity of ionic-liquid membranes [20]. Melamine is a particularly intriguing amine crosslinker based on the remarkably high interaction energy with CO_2 observed in, density functional theory (DFT) computational studies [21].

In this study, we used computational modelling to propose melamine-crosslinked PEG membranes for $(H_2S+CO_2)/CH_4$ and H_2S/CO_2 separations. We then synthesized crosslinked PEG membranes using azide-alkyne cycloaddition click chemistry and tested their properties under sour and acid mixed gas feeds for CO_2/CH_4, H_2S/CH_4, and H_2S/CO_2 separations. Additionally, we observed the effect of various PEG chain lengths (molecular weights 200-1000 g/mol) on physical, thermal and gas separation properties of the membranes. In conclusion, we found that the incorporation of melamine crosslinkers in membrane has the potential to allow for efficient H_2S/CO_2 separations.

2. Materials, Instrumentation and Experimental Methods

2.1. Materials

Cyanuric fluoride, propargylamine 98%, bromotris(triphenylphosphine)copper(I), and tetrahydrofuran (THF) anhydrous (99.9% inhibitor free) were purchased from Sigma Aldrich. The monomers poly(ethylene glycol)bisazide (PEG_{1100}-bisazide, M_n =1100, Sigma Aldrich), azide-PEG-azide (PEG_{600}-bisazide, M_n = 600, Creative PEGWorks), 1,17-Diazido-3,6,9,12,15-pentaoxaheptadecane (PEG_{332}-bisazide, m.w. = 332, Sigma Aldrich), 1,11-Diazido-3,6,9-trioxaundecane (PEG_{224}-bisazide, m.w. = 244, Sigma Aldrich), PEG-di-*p*-tosylate (PEG_{1800}-ditosylate, M_n = 1800, Sigma Aldrich), and poly(ethylene glycol) diglycidyl ether (PEG_{500}-diglycidyl ether, M_n = 500, Sigma Aldrich) were used as received. The polytetrafluoroethylene (PTFE) evaporating dishes were purchased from Thermo Fisher Scientific.

2.2. Instrumentation

^{1}H-NMR (500 MHz) spectra were obtained with a Bruker Ascend 500 MHz spectrometer with samples dissolved in DMSO-d_6. NMR tubes were cleaned with a 3D-printed NMR tube cleaner [22]. Thermographic analysis (TGA, TA Instruments TGA1-0280) was completed using a ramp of 10 °C/min to 850 °C under nitrogen. Differential calorimeter analysis (DSC, TA Instrument DSC1-0303) was executed on the membranes with parameters of heating to 100 °C at 10 °C/min, cooled at -80 °C at 10 °C/min and reheating to 100 °C ramped at 10 °C/min. Fourier transform infrared (FTIR) spectra were collected on a Thermo Scientific Nicolet iS50 with attenuated total reflectance (ATR) capabilities. Gas permeation testing was performed through a custom-designed constant-volume permeation cell system [23]. The membrane was placed in a sealed cell and vacuum was applied overnight prior to recording data. A Shimadzu GC equipped with a thermal conductivity detector was used to determine the permeate mixture. An Isco pump (Teledyne Isco) was used to control the gas feed pressure up to 55.2 bar. Mixed gas cylinders were received from Matheson Tri-Gas and Airgas.

2.3. Computational Details

The free membrane model components were optimized using XTBDFT, a multi-level algorithm using GFN2-xTB and CREST for initial conformer generation and sorting and density functional theory (DFT) as implemented in NWChem 6.8 to refine geometries and electronic energies [24-26]. Initial DFT geometry refinement used the B97 functional with Grimme D3 semi-empirical dispersion correction and def2-SVP basis set, and high-level electronic energy was computed with the same functional and dispersion correction but the larger def2-TZVP basis set [27-29]. To model gas permeate molecules (CO_2 or H_2S) binding to the membrane, the same workflow was used, except that the CREST calculation used the "-nci" flag to apply an ellipsoidal potential around the input structure to help search for non-covalent interaction conformers. Binding energy (ΔE_{int}) is calculated as the difference in high-level electronic energies between the membrane-bound permeate versus the free membrane and free permeate molecules.

2.4. Synthesis of trispropargylmelamine crosslinker

A round bottom flask was flame dried under flowing nitrogen to remove any water. Cyanuric fluoride is water-reactive, toxic, and volatile, and were only used inside a fume hood under inert gas. Propargylamine is a highly flammable, volatile liquid only to be used under the fume hood under inert gas. Both PHS chemicals were handled with polyvinyl chloride (PVC) gloves over a layer of nitrile gloves with a lab coat and goggles. Cyanuric fluoride 1.0 g (1.0 eq.) was dissolved in 77.5 mL of toluene. The mixture was stirred and refluxed while 4.69 mL (6.3 eq.) of propargylamine was added dropwise. The solution was kept at reflux for 16 h, during which red powder deposited on the sides of the round bottom flask. A hot filtration was filtered through a vacuum filter and washed with toluene to obtain a yellow filtrate, which was placed into an ice bath overnight. After 24 h, a yellow precipitate was collected. (Yield = 91%) ^{1}H-NMR (500 MHz, $(CD_3)_2SO$): δ 7.1 (m, N-*H*, 3H), 3.98 (m, C*H*$_2$, 6H), 3.0 (s, C≡C-*H*, 3H) (Fig. S4.1). Efforts to substitute cyanuric fluoride with less toxic cyanuric chloride resulted in only 4% isolated yield, with substantial amounts of mono-, and di-propargyl intermediates observed in the product mixture by ^{1}H-NMR and gas chromatography-mass spectrometry (GC-MS).

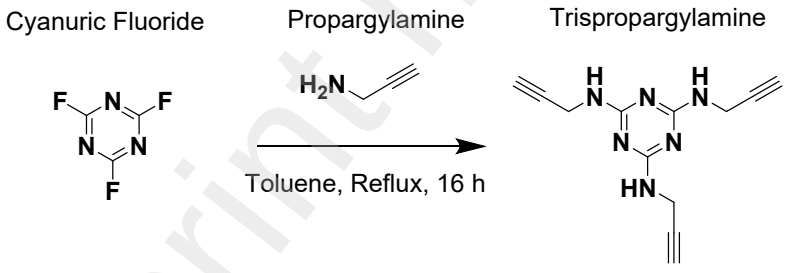

Fig. 1. Schematic representation of the synthesis of the trispropargylmelamine (melamine-based crosslinker) [30-33].

2.5. Synthesis of MEL-PEG Membrane

The membrane was formed through copper-catalyzed click chemistry using an azide-alkyne reaction. In an empty vial, the copper catalyst, bromotris(triphenylphosphine)copper(I) (0.2wt%), trispropargylmelamine crosslinker (1 mol eq.), and PEG-bisazide (1.5 mol eq.) were dissolved in

tetrahydrofuran (THF) at ambient temperature. The solution was filtered through a PTFE syringe filter (0.45µm) and cast on a level plate in a PTFE evaporating dish. After exploring many process variables to obtain suitable membranes, the MEL-PEG_{1100} and MEL-PEG_{600} were cast inside a nitrogen-filled glove bag (Thermo Scientific, AAA91717-LK) saturated with THF vapor, while MEL-PEG_{332} and MEL-PEG_{224} were cast under ambient conditions outside the glove bag and covered with a glass dish. The membranes were left overnight to dry. All membranes were then heated at 80 °C under vacuum for 24 h in the PTFE dish. The thicknesses of the membrane dense films were measured with a micrometer to be between 50µm-100µm (Fig. S3.1). Experimental details and further characterization can be found in the Supporting Information (Appendix S4).

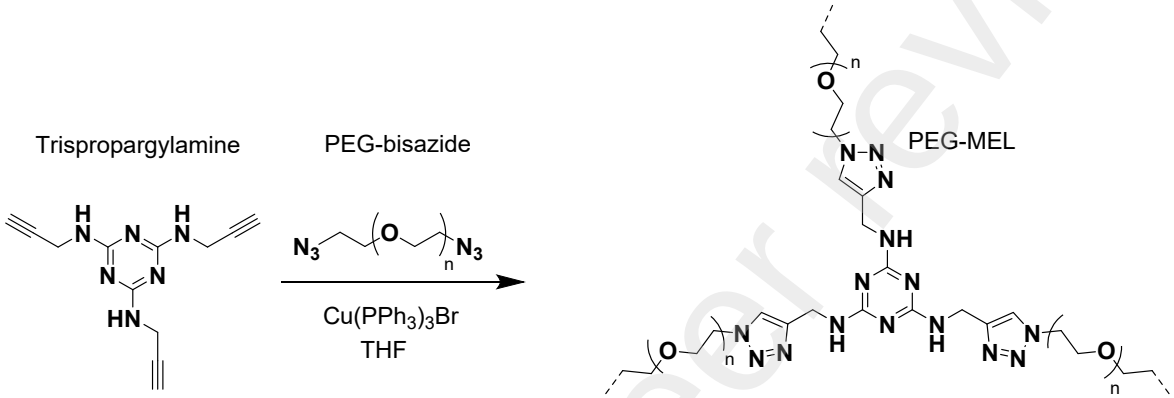

Fig. 2. Schematic representation of the synthesis of PEG-MEL membranes

Table 1. Membrane Synthesis Parameters

Membrane	Casting Surface (60mm Diameter)	PEG: Crosslinker (molar ratio)	PEG: Crosslinker: $Cu(PPh_3)_3Br$ (mass fraction %)	Membrane Thickness (µm)
MEL-PEG_{1100}	Evaporating PTFE Dish	1.5:1	86:13:1	72
MEL-PEG_{600}			78:21:1	58
MEL-PEG_{332}			63:34:3	70
MEL-PEG_{244}			55:42:3	80

3. Results and Discussion

3.1. Molecular Design

Computational models were used to rationally improve upon the H_2S/CO_2 selectivity of our previously reported PTI-crosslinked PEG membranes [14]. Given the conformationally flexible nature of the various polymer components, XTBDFT was used to efficiently explore binding modes of H_2S and CO_2 and calculate binding energies for the minimum-energy conformers [24, 34]. Triglyme was used as a truncated model of the majority PEG domains, and H_2S binding (-7.5 kcal/mol) is preferred over CO_2 binding (-4.6 kcal/mol) by 2.9 kcal/mol (Fig. 3, right). The PTI crosslinker was modelled with two ethylene oxide repeat units per carbamate arm. In comparison to triglyme, the binding energies of PTI with H_2S and CO_2 (-9.2 and -6.5 kcal/mol, Fig. 3, middle) are higher, but the affinity for H_2S over CO_2 is smaller (2.7 kcal/mol). This agrees with the prior experimental result of worse $\alpha(H_2S/CO_2)$ with higher PTI/PEG weight ratio.

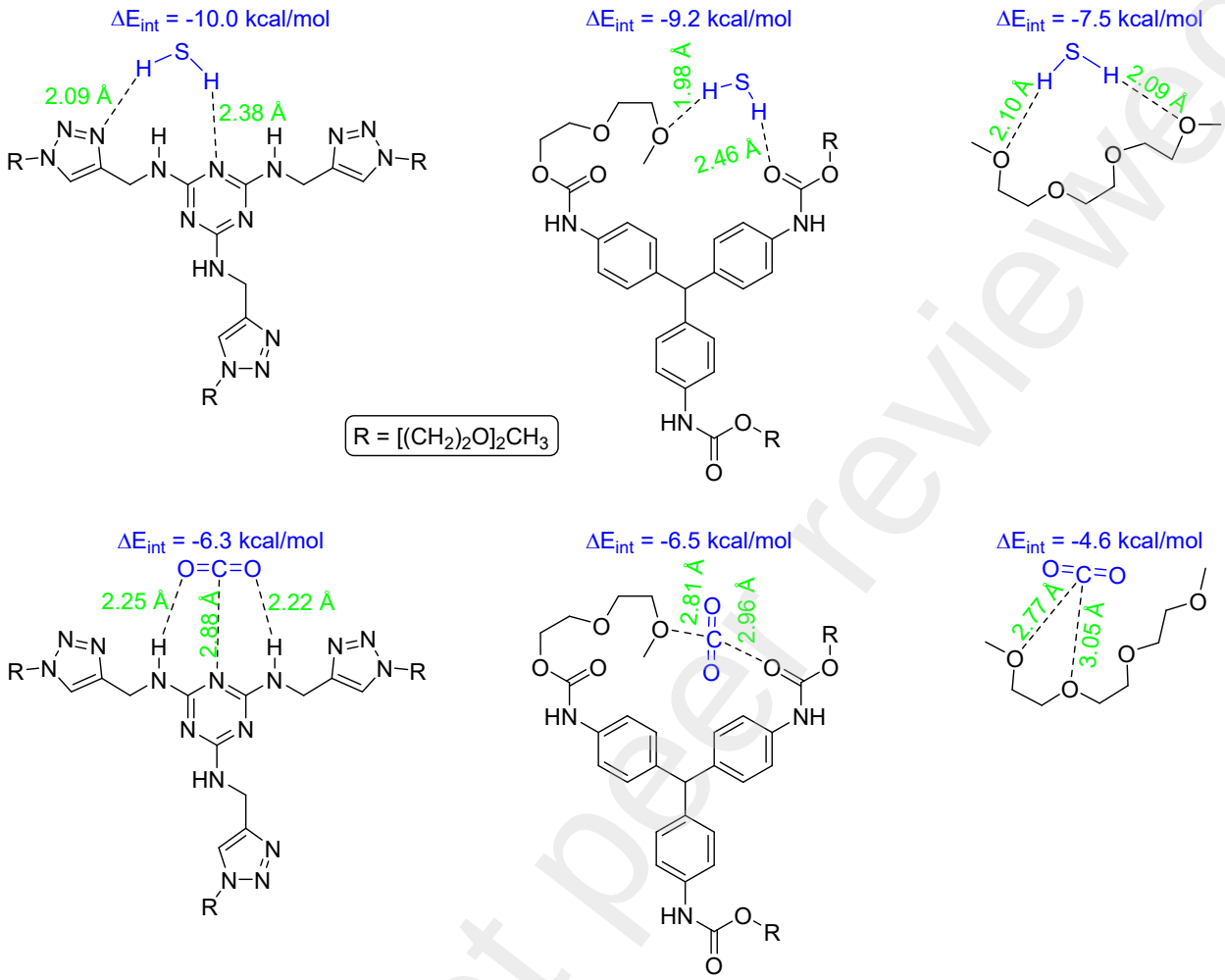

184

185 **Fig. 3.** Binding geometries and energies for H_2S (top) and CO_2 (bottom) with various polymer components.
186 Selected intermolecular distances are labeled.

187 Melamine was considered as an alternative crosslinker given its theoretically exceptional affinity
188 for CO_2 due to its dense and rigid arrangement of Lewis acid and base sites [21]. While PEG-
189 diglycidyl ether and PEG-ditosylate have been successfully crosslinked with other triamines, our
190 experimental efforts to directly use melamine as the crosslinker under analogous reaction
191 conditions did not yield intact films [35, 36]. The amines of melamine are deactivated by the
192 electron-poor triazine ring, and likely prevent efficient nucleophilic substitution crosslinking
193 reactions. To more efficiently utilize melamine crosslinkers, N,N',N"-trispropargylmelamine was
194 synthesized from cyanuric fluoride and propargyl amine in high yield, and envisioned to be able
195 to react with bisazide-functionalized PEG (PEG-bisazide) under mild conditions via azide-alkyne
196 cycloaddition click chemistry [37]. Before optimizing the various interrelated process conditions
197 for casting crosslinked membranes (Appendix S3 of the SI), computational models were used to
198 predict the H_2S/CO_2 binding affinity of the melamine crosslinker with two ethylene oxide repeat
199 units per triazole arm (Fig. 3, left). H_2S binds through two hydrogen bonds, one to the central
200 triazine and one to a triazole, with a binding energy of 10.0 kcal/mol. CO_2 binds to the melamine
201 core via two hydrogen bonds and a weak C-N Lewis acid-base type interaction, with a binding

energy of 6.3 kcal/mol. The large preference for binding H_2S over CO_2 (3.7 kcal/mol) indicates that H_2S/CO_2 selectivity of such melamine-crosslinked membranes should be higher than for membranes composed of pure PEG or PTI-PEG.

3.2. Synthesis of MEL-PEG membranes

PEG-bisazide and trispropargylamine were crosslinked using azide-alkyne click chemistry using a Cu(I) catalyst and THF solvent. Several interrelated process variables were systematically varied to cast satisfactory crosslinked membranes: solvent evaporation rate, concentration of polymer solution, and casting substrate (Appendix S3 of the SI). Many casting conditions resulted in non-uniform, overly fragile, or otherwise not castable polymeric membranes. The optimized conditions for casting MEL-PEG_{1100} and MEL-PEG_{600} membranes on PTFE evaporating dishes required enclosure in a glove bag saturated with THF vapor to slow down solvent evaporation rate and obtain a uniform membrane. MEL-PEG_{332} and MEL-PEG_{244} membranes were optimally cast enclosed under a glass petri dish cover. Attempts to cast MEL-PEG_{332} and MEL-PEG_{244} inside a glove bag resulted in non-uniform membranes due to slow evaporation rate. MEL-PEG_{332} and MEL-PEG_{244} membranes crosslinked quicker trapping the solvent in the membrane causing visible surface defects.

3.3. Membrane Characterization

MEL-PEG membranes were characterized by FTIR spectroscopy (Fig. 4a) to ensure that the PEG-bisazide and functionalized melamine-based crosslinker reacted completely. FTIR spectra showed an increase in the -NH bend at 1500 cm^{-1} as the PEG molecular weight decreases (Fig. 4b). MEL-PEG_{332} and MEL-PEG_{244} membranes contain shorter linear PEG chains which require more integration of the crosslinker to form the membranes. This results in a higher amine content present in the overall polymer matrix. The FTIR spectra exhibit broad peaks at 1000-1200 cm^{-1} that are attributed to C-O stretching from the PEG chains. This peak decreases as PEG molecular weight deceases due to the fewer C-O bonds per crosslinker. MEL-PEG membranes exhibit no peaks at ~2100 and 3400 cm^{-1} indicating the elimination of azide ($N^-=N^+=N^-$) and alkyne (C≡C-H) peaks, thus confirming successful integration of the melamine crosslinker with the PEG monomers.

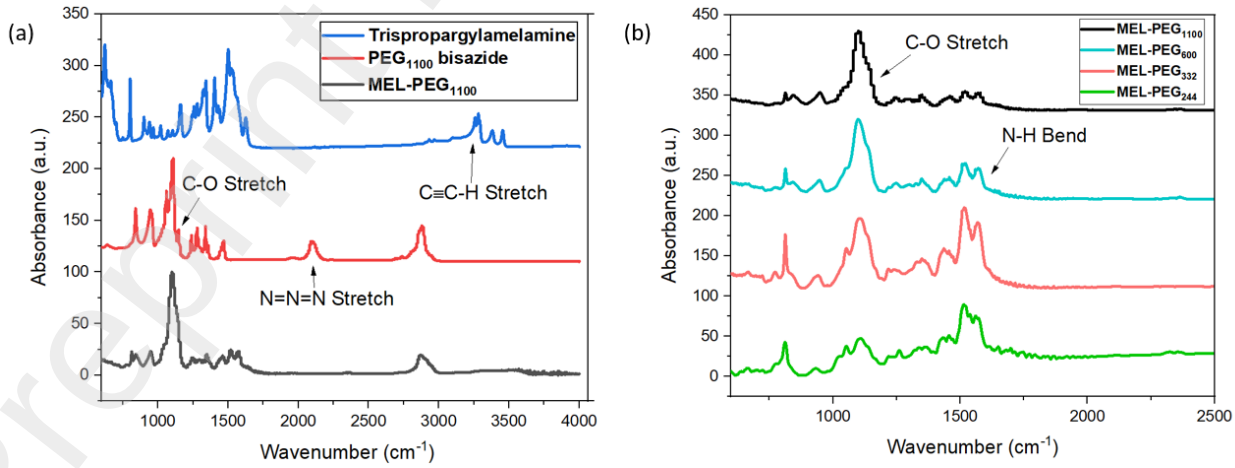

Fig. 4. (a) FTIR spectra of starting materials PEG_{1100}-bisazide and trispropargylamelamine compared to MEL-PEG membrane (b) FTIR spectra of crosslinked MEL-PEG membranes

The MEL-PEG membranes are thermally stable up to 200 °C. Glass transition and degradation temperatures are listed in Table 2. Further TGA and DSC graphs can be found in the Supporting Information (Fig. S4.2).

Table 2. Glass transition (T_g) and decomposition temperature (T_d) measured by DSC and TGA

membranes	**decomposition temperature T_d(°C)**			**T_g (°C)**
	T_{d5}	**T_{d10}**	**T_{d20}**	
MEL-PEG$_{1100}$	333.6	368.6	383.0	-47.8
MEL-PEG$_{600}$	328.6	366.5	380.7	-28.9
MEL-PEG$_{332}$	258.3	347.4	373.9	-3.9
MEL-PEG$_{244}$	222.3	319.9	370.9	2.8

MEL-PEG membranes such as MEL-PEG$_{332}$ and MEL-PEG$_{244}$ with shorter linear polymer chain lengths exhibit higher T_g due to the incorporation of more crosslinker. The addition of the crosslinker results in a decrease of the overall polymeric chain mobility and fractional free volume. The shorter PEG oligomers (< 332 g/mol) form glassy membranes that are brittle, rigid, and fragile. Longer PEG oligomers (> 600 g/mol) form rubbery membranes that are more flexible and robust. Crosslinking the membranes impacts chain rigidification and is well known to have an influence on the permeation transport properties, in particular the balance between selectivity and permeability.

3.4. Pure Gas Permeation

Pure gas CO_2 and CH_4 permeation tests were performed at 6.9 bar to ensure no defects in the membranes and to investigate the impact of the molecular weight in correlation to permeability and selectivity (Fig. 5). Membranes derived from the lower PEG linear molecular weight chains were brittle and glassy, and exhibited an increase in CO_2/CH_4 selectivity, but significantly decreased CO_2 permeability. Overloading of melamine crosslinker negatively impacted the membrane by decreasing permeability and membrane robustness. Membranes derived from higher molecular weight PEG chains produced a more robust rubbery and flexible membrane that showed a substantial increase in CO_2 permeability while retaining an attractive CO_2/CH_4 selectivity. In contrast, PTI-PEG membranes derived from PEG precursors of the same molecular weight exhibited drastically lower overall permeabilities and similar CO_2/CH_4 selectivities (Table 3). Notably, the near identical CO_2/CH_4 selectivities of MEL-PEG and PTI-PEG are consistent with the very similar DFT-calculated interaction energies of the respective crosslinkers with CO_2 (-6.3 and -6.5 kcal/mol, Figure 4), supporting the utility of DFT calculations for designing gas separation membranes. The most promising membranes consisted of the higher PEG molecular weight chains (MEL-PEG$_{1100}$ and MEL-PEG$_{600}$) due to more attractive tradeoff between selectivity and permeability. Therefore, these membranes were further tested under binary and mixed gas conditions. Permeation calculations are outlined in Supporting Information Appendix S4.

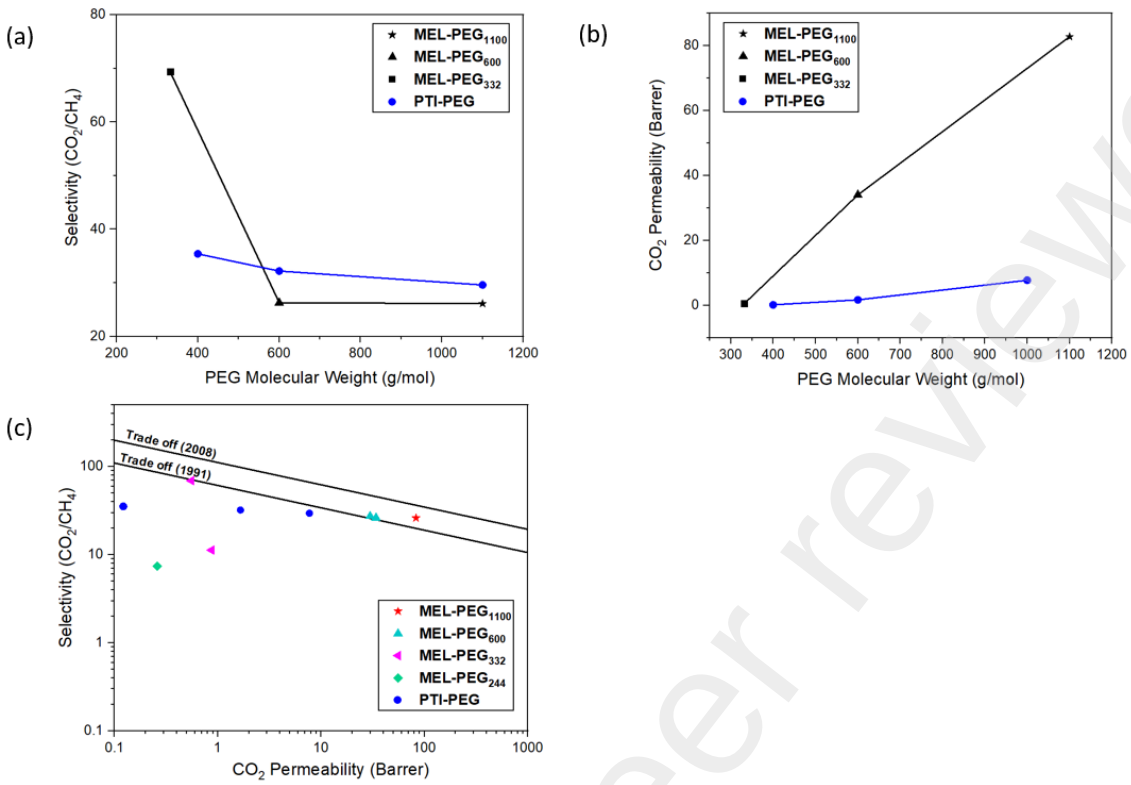

Fig. 5. (a) CO_2/CH_4 selectivity as a function of PEG molecular weight (b) CO_2 permeability as a function of PEG molecular weight (c) Pure gas (CO_2 and CH_4) permeation of MEL-PEG membranes compared to PTI-PEG membranes at 6.9 bar

Table 3. Pure Gas Permeation at 6.9 bar at room temperature

Crosslinked Membranes	**CO_2 Permeability (Barrer)**	**CH_4 Permeability (Barrer)**	**Selectivity CO_2/CH_4**
MEL-PEG_{1100}	82.8 ± 3	3.2 ± 0.2	25.9 ± 0.6
MEL-PEG_{600}	34.1 ± 5	1.1 ± 0.2	27.1 ± 1.1
PTI-PEG_{1000}	7.7 ± 3.6	0.2 ± 0.01	29.6 ± 1.8
PTI-PEG_{600}	0.06 ± 0.01	1.7 ± 0.13	32 ± 4.8

3.5. Mixed Gas Permeation

Binary CO_2-CH_4 gas permeation testing was conducted on MEL-PEG_{1100} and MEL-PEG_{600} membranes at room temperature and pressures up to 55.2 bar. The MEL-PEG_{1100} membrane yielded the most attractive permselectivity, yielding a CO_2/CH_4 selectivity of ~26 and a CO_2 permeability of ~78 Barrer, matching the performance metrics of MEL-PEG_{1100} under pure gas permeation conditions at 6.9 bar (Table 3). Interestingly, changing the feed pressure (13.8 to 55.2 bar), did not greatly affect the permeability and selectivity of these membranes. Additional details for binary gas testing can be found in the Supporting Information (Fig. S5.1 and Table S5.2).

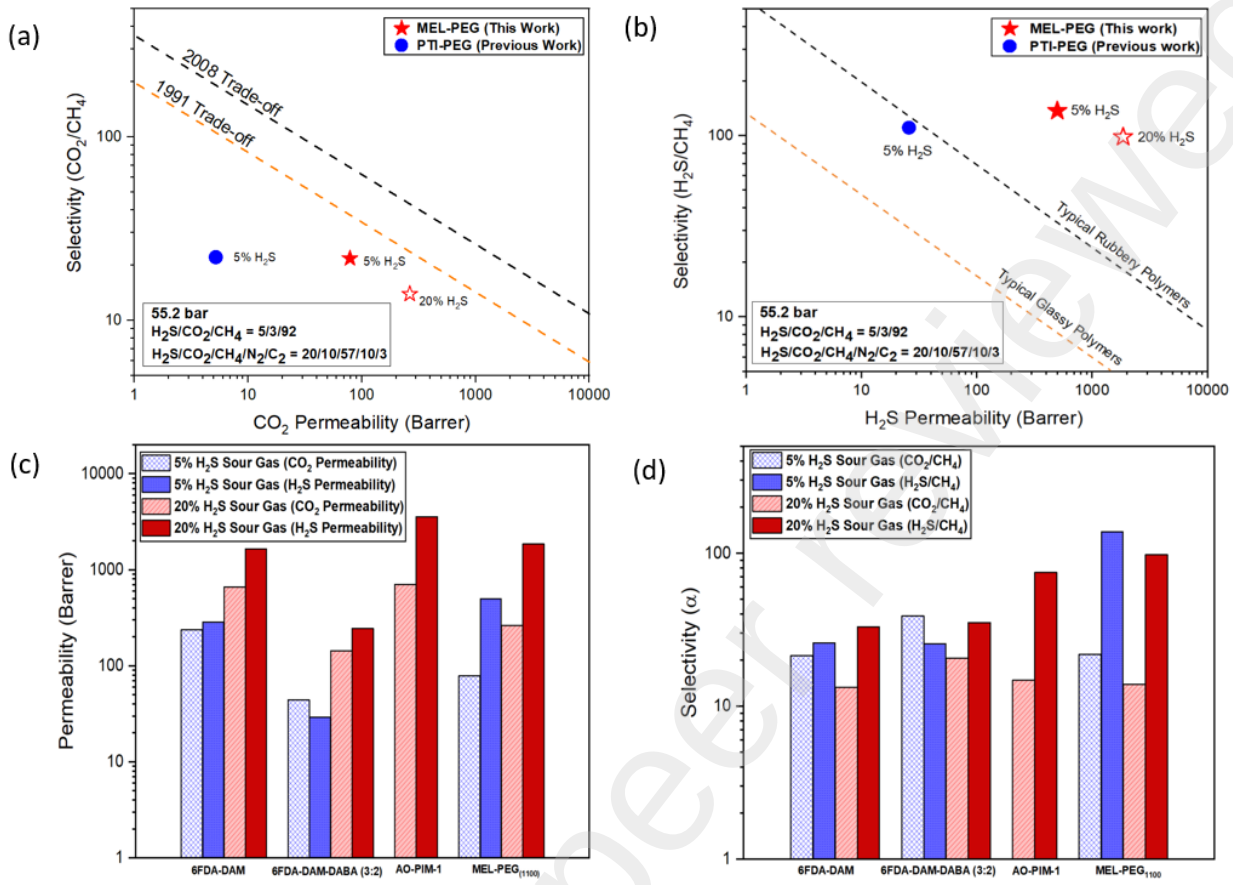

Fig. 6. MEL-PEG$_{1100}$ mixed gas testing results (a) CO_2/CH_4 selectivity compared to PTI-PEG$_{1000}$ membrane (b) H_2S/CH_4 selectivity compared to PTI-PEG membrane (c) H_2S and CO_2 permeability compared to common benchmark membranes (d) H_2S/CH_4 and CO_2/CH_4 selectivity compared to common benchmark membranes. Mixed gas composition: (i) 5% H_2S, 3% CO_2, 92% CH_4 and (ii) 20% H_2S, 10% CO_2, 57% CH_4, 10% nitrogen (N_2), 3% ethane (C_2H_6).

Simulated sour gas permeation tests were performed with MEL-PEG$_{1100}$ at high pressure (55.2 bar) with two mixed gas feeds: (a) low acid gas - 5% H_2S, 3% CO_2, 92% CH_4 and (b) high acid gas - 20% H_2S, 10% CO_2, 57% CH_4, 10% N_2, 3% C_2H_6. MEL-PEG$_{1100}$ exhibited improved H_2S/CH_4 selectivity and nearly identical CO_2/CH_4 selectivity compared to PTI-PEG$_{1000}$ membranes (Figs. 5a, b). These results agreed with our initial DFT calculations, which showed that the MEL crosslinker binds H_2S more strongly than PTI crosslinker (-10.0 vs -9.2 kcal/mol, Fig. 3), but that the two crosslinkers exhibit similar CO_2 binding energies (-6.3 and -6.5 kcal/mol, Fig. 3. Additionally, MEL-PEG$_{1100}$ exhibited improved H_2S and CO_2 permeability in mixed gas condition compared to the PTI-PEG membranes.

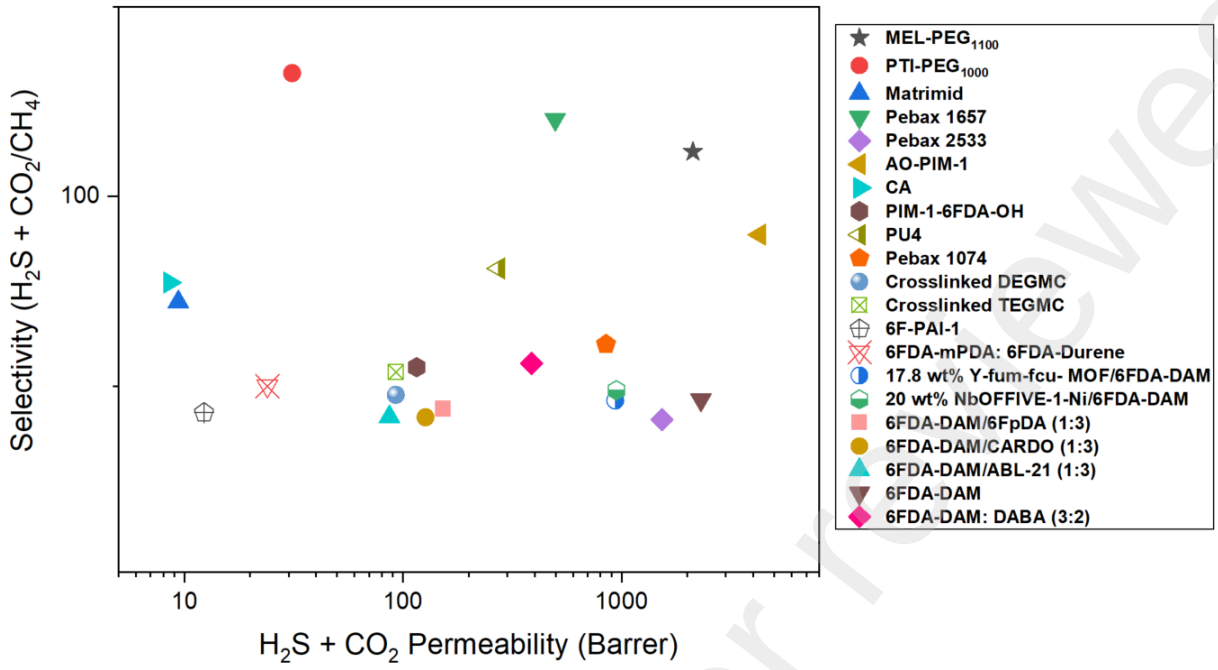

Fig. 7. Comparison to other rubbery and glassy polymeric membranes under H_2S and CO_2 mixed gas feeds.

Common benchmark polyimide membranes 6FDA-DAM and 6FDA-DAM: DABA (3:2) were fabricated [38-41] and tested with low and high acid gas concentration feeds to compare with the MEL-PEG$_{1100}$ membrane. MEL-PEG$_{1100}$ has CO_2 and H_2S permeabilities above 100 Barrer (Fig. 6c) but the CO_2/CH_4 selectivity was relatively low (Fig. 6d). Notably, MEL-PEG$_{1100}$ exhibited remarkably higher H_2S/CH_4 selectivity than the benchmark polyimide membranes [42, 43]. There was a noticeable difference between H_2S/CH_4 and CO_2/CH_4 selectivities due to the abundance of N-heterocycles and secondary amines in the MEL-PEG$_{1100}$ membrane that preferentially interact with H_2S interactions over CO_2. Compared to various membranes across the literature (Fig. 7), MEL-PEG$_{1100}$ is one of the best performing materials tested for combined (H_2S + CO_2)/CH_4 selectivity at room temperature and for combined (H_2S + CO_2) permeability.

Table 4. The plasticization effects on membrane selectivity under 5% and 20% H_2S sour mixed gas feeds at pressures of 55.2 bar.

Membrane	P $_{(CO2+H2S)}$ 5% H_2S	P $_{(CO2+H2S)}$ 20% H_2S	ΔP $_{(CO2+H2S)}$	α $_{(H2S+CO2)/CH4}$ 5% H_2S	α $_{(H2S+CO2)/CH4}$ 20% H_2S	Δα $_{(H2S+CO2)/CH4}$
6FDA-DAM*	525.6	2310.9	339.7%	47.5	46.4	-2.3%
6FDA-DAM: DABA (3:2)*	73.5	388.1	388.1%	64.7	56	-13.4%
MEL-PEG$_{1100}$	579.5	2123.9	266.5%	161	111.8	-30.6%

All membranes were tested under 55.2 bar.
**6FDA-DAM and 6FDA-DAM: DABA (3:2) were cast and annealed at 200 °C under vacuumed for 24h.*

Gas separation membranes often swell and exhibit higher permeability, but lower selectivity at higher concentrations of acid gases. This effect is often attributed to plasticization, where polymer chains lose local interchain interactions under high concentrations of permeate [42]. We studied the effect of plasticization by comparing membranes' performance at high pressure (55.2 bar) with

the low acid gas and high acid gas feed compositions described above. Upon switching from low to high acid gas concentration, MEL-PEG_{1100} exhibited a 30.6% decrease in selectivity ($\Delta\alpha_{(H2S+CO2)/CH4}$) and 266.5% increase in H_2S and CO_2 permeability ($\Delta P_{CO2+H2S}$) in Table 4, row 3. This suggests that MEL-PEG_{1100} membranes undergo plasticization, despite its crosslinked structure. Long, conformationally flexible PEG_{1100} segments retain local mobility, and the overall material is not made plasticization-resistant by the melamine crosslinkers. In contrast, benchmark glassy polyimides like 6FDA-DAM and 6FDA-DAM: DABA (3:2) have less loss of $(H_2S+CO_2)/CH_4$ selectivity and more increase in permeation when switching from low to high acid gas concentrations (Table 4, rows 1-2). Their better plasticization resistance is due to their rigid polymer backbones comprised of conjugated rings and quaternary carbons. that limits loss of interchain contacts [44]. Additional details on mixed gas permeation can be found in Table S5.3. The MEL-PEG_{1100} membrane was further tested for H_2S/CO_2 selectivity in mixed gas feed conditions at lower pressures for acid gas enrichment.

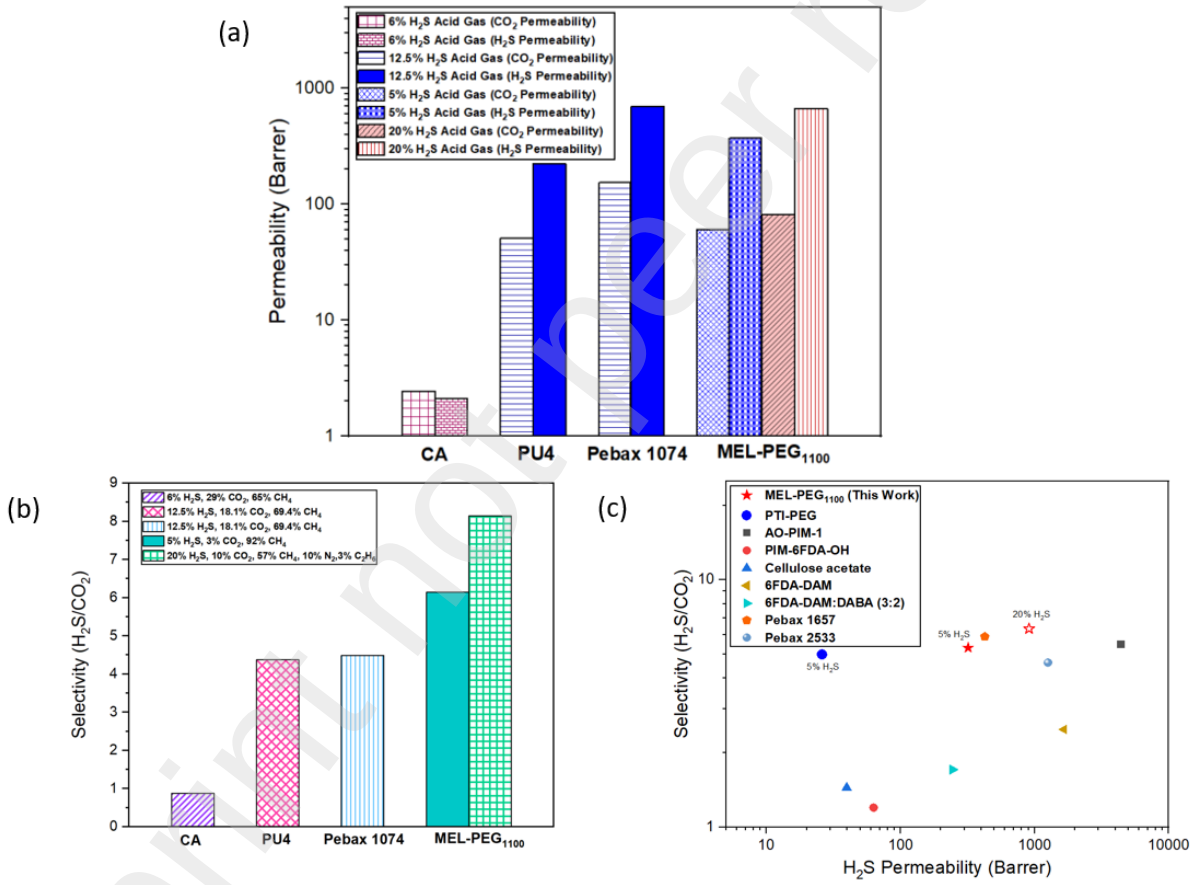

Fig. 8. Summary of mixed gas permeation and selectivity tests of MEL-PEG membranes at low pressure (a) Comparison of other polymeric membranes under H_2S and CO_2 mixed gas feeds at 10.3 bar investigating the H_2S permeability (b) Comparison of other polymeric membranes under H_2S and CO_2 mixed gas feeds at 10.3 bar investigating the H_2S/CO_2 selectivity (c) Compiled list of H_2S permeability and H_2S/CO_2 selectivity in comparison to other polymeric membranes. Additional references for the polymeric membranes are in the Supporting Information Table S5.3.

Acid gas enrichment focuses on separating H_2S from CO_2 in a downstream processing step where feed pressure is typically lower than the pressure used in AGR separations. In this separation, the MEL-PEG_{1100} showed increased CO_2 and H_2S permeabilities, likely due to the higher concentration of plasticizing H_2S gas (Fig. 8a). The MEL-PEG_{1100} selectivity in Fig. 8b outperformed most polymeric membranes measured under similar mixed gas conditions. Fig. 8c illustrated how MEL-PEG_{1100} membrane demonstrated better H_2S/CO_2 selectivity compared to other rubbery polymers including poly(ether urethane urea) PU4, cellulose acetate (CA) and Pebax 1074 while maintaining good H_2S permeability (> 300 Barrer) in mixed gas feeds containing 20% H_2S [42, 45]. Notably, the MEL-PEG_{1100} membrane maintained the most attractive H_2S/CO_2 selectivity between 6.1-8.1. When applied to rubbery membranes, the solution-diffusion mechanism tends to rely more on the sorption-selectivity factor instead of the diffusion-selectivity factor. Our computationally designed melamine crosslinker favors sorption of H_2S over CO_2, resulting in faster permeability of H_2S through the membrane and provides rationale as to why this material emerged as a top performer in this evaluation. Further details of the H_2S/CO_2 separations can be found in Supplementary Information Table S5.3.

4. Conclusions

In summary, a novel melamine-based crosslinker was designed using DFT calculations to enhance the H_2S and CO_2 selectivity of PEG-based gas separation membranes. Various PEG molecular weights (≤1100 g/mol) with the novel melamine crosslinker were successfully synthesized via azide-alkyne cycloaddition click chemistry. MEL-PEG_{1100} demonstrated good CO_2/CH_4 performance out of the MEL-PEG membranes under pure and binary gas conditions. Under mixed gas conditions (up to 20% H_2S) the MEL-PEG_{1100} resulted in best H_2S permeabilities and H_2S/CO_2 selectivity.

This extensive testing highlighted how membrane performance can be affected by high concentrations of 20% H_2S gas under high and low pressures. Overall, these results show that the functionalized melamine crosslinker helped improve H_2S and CO_2 permeability by improving the PEG membrane sorption properties. Ultimately, we found that MEL-PEG_{1100} can be a potential candidate for CO_2/CH_4 and H_2S/CH_4 gas separations but is primarily attractive for H_2S/CO_2 separation. This performance all derives from correlation between computationally guided design of the melamine crosslinker and enhanced H_2S sorption in the membrane.

Declaration of competing interest

The authors declare that they have no known competing financial interests or personal relationships that could have appeared to influence the work reported in this paper.

CRediT authorship contribution statement

Dana A. Wong: Methodology, Investigation, Data Curation, Writing - original draft. **Elizabeth E. Haddad:** Investigation, Validation, Writing - original draft. **Sibo Lin:** Software, Writing - original draft, Writing - review & editing. **Seth A. Sharber:** Methodology, Investigation. **John Yang:** Writing - review & editing. **Daniel J. Harrigan:** Conceptualization. **John A. Lawrence:** Conceptualization. **Patrick T. Wright:** Investigation. **Yang Liu:** Investigation, Writing - review

& editing. **Benjamin J. Sundell:** Conceptualization, Project administration, Writing - review & editing.

Acknowledgments

Authors acknowledge helpful discussions with Sipei Li, Brian Hanna and Michael Forte. This project solely used funding from our industrial organization (Aramco/Aramco Services Company).

Appendix A. Supplementary Material

Supplementary data to this article can be found online at

References

[1] H. Ritchie, P. Rosado, Energy Mix, (2022) https://ourworldindata.org/energy-mix.
[2] G. George, N. Bhoria, S. AlHallaq, A. Abdala, V. Mittal, Polymer membranes for acid gas removal from natural gas, Sep. Purif. Technol. 158 (2016) 333.
[3] U.S. Energy Information Administration, U.S. natural gas production and LNG exports will likely grow through 2050 in AEO2023 (2023).
[4] N.W. Chakroun, A.F. Ghoniem, Techno-economic assessment of sour gas oxy-combustion water cycles for CO2 capture, Int. J. Greenhouse Gas Control 36 (2015) 1.
[5] T.N.A. Tengku Hassan, A.M. Shariff, M.M.i. Mohd Pauzi, M.S. Khidzir, A. Surmi, Insights on Cryogenic Distillation Technology for Simultaneous CO2 and H2S Removal for Sour Gas Fields, Molecules 27 (2022) 1424.
[6] D. Perry, R. Fedich, L. Parks, Better acid gas enrichment, Sulphur 326 (2010) 38.
[7] A.J. Kidnay, W.R. Parrish, D.G. McCartney, Fundamentals of natural gas processing, CRC Press Boca Raton, FL (2011) 574.
[8] H.R. Mahdipoor, A. Dehghani Ashkezari, Feasibility study of a sulfur recovery unit containing mercaptans in lean acid gas feed, J. Nat. Gas Eng. 31 (2016) 585.
[9] A.A. Abd, M.R. Othman, Z. Helwani, J. Kim, Waste to wheels: Performance comparison between pressure swing adsorption and amine-absorption technologies for upgrading biogas containing hydrogen sulfide to fuel grade standards, Energy 272 (2023) 127060.
[10] R.W. Baker, K. Lokhandwala, Natural gas processing with membranes: an overview, Ind. Eng. Chem. Res. 47 (2008) 2109.
[11] S.R. Reijerkerk, M.H. Knoef, K. Nijmeijer, M. Wessling, Poly(ethylene glycol) and poly(dimethyl siloxane): Combining their advantages into efficient CO2 gas separation membranes, J. Membr. Sci. 352 (2010) 126.
[12] A. Kargari, S. Rezaeinia, State-of-the-art modification of polymeric membranes by PEO and PEG for carbon dioxide separation: A review of the current status and future perspectives, J. Ind. Eng. Chem 84 (2020) 1.
[13] Z. Tong, A.K. Sekizkardes, Recent Developments in High-Performance Membranes for CO2 Separation, Membranes (2021) 156.
[14] D.J. Harrigan, J.A. Lawrence, H.W. Reid, J.B. Rivers, J.T. O'Brien, S.A. Sharber, B.J. Sundell, Tunable sour gas separations: Simultaneous H2S and CO2 removal from natural gas via crosslinked telechelic poly(ethylene glycol) membranes, J. Membr. Sci. 602 (2020) 117947.
[15] A. Ghadimi, R. Gharibi, H. Yeganeh, B. Sadatnia, Ionic liquid tethered PEG-based polyurethane-siloxane membranes for efficient CO2/CH4 separation, Mater. Sci. Eng., C 102 (2019) 524.

[16] J. Deng, J. Yu, Z. Dai, L. Deng, Cross-Linked PEG Membranes of Interpenetrating Networks with Ionic Liquids as Additives for Enhanced CO2 Separation, Ind. Eng. Chem. Res. 58 (2019) 5261.
[17] H. Xu, S.G. Pate, C.P. O'Brien, The influence of amine structure on the mechanism of CO2 facilitated transport across amine-functionalized polymer membranes: An operando spectroscopy study, J. Membr. Sci. 689 (2024) 122163.
[18] T. Yamaguchi, L.M. Boetje, C.A. Koval, R.D. Noble, C.N. Bowman, Transport Properties of Carbon Dioxide through Amine Functionalized Carrier Membranes, Ind. Eng. Chem. Res. 34 (1995) 4071.
[19] C.N. Okonkwo, C. Okolie, A. Sujan, G. Zhu, C.W. Jones, Role of Amine Structure on Hydrogen Sulfide Capture from Dilute Gas Streams Using Solid Adsorbents, Energy Fuels 32 (2018) 6926.
[20] L. Peng, M. Shi, X. Zhang, W. Xiong, X. Hu, Z. Tu, Y. Wu, Facilitated transport separation of CO2 and H2S by supported liquid membrane based on task-specific protic ionic liquids, Green ChE 3 (2022) 259.
[21] H.M. Lee, I.S. Youn, M. Saleh, J.W. Lee, K.S. Kim, Interactions of CO2 with various functional molecules, Phys. Chem. Chem. Phys. 17 (2015) 10925.
[22] D.A. Wong, S. Lin, A 3D-Printed Higher-Throughput NMR Tube Cleaner, J. Lab. Chem. Educ. 9 (2021) 37.
[23] J. Vaughn, D. Harrigan, B. Sundell, J. Lawrence Iii, J. Yang, Reverse Selective Glassy Polymers for C3+ Hydrocarbon Recovery from Natural Gas, J. Membr. Sci. 522 (2016) 68.
[24] S. Lin, M. Elanany, M. Khawaji, XTBDFT: Automated workflow for conformer searching of minima and transition states powered by extended tight binding and density functional theory, SoftwareX 20 (2022) 101242.
[25] P. Pracht, F. Bohle, S. Grimme, Automated exploration of the low-energy chemical space with fast quantum chemical methods, Phys. Chem. Chem. Phys. 22 (2020) 7169.
[26] M. Valiev, E.J. Bylaska, N. Govind, K. Kowalski, T.P. Straatsma, H.J.J. Van Dam, D. Wang, J. Nieplocha, E. Apra, T.L. Windus, W.A. de Jong, NWChem: A comprehensive and scalable open-source solution for large scale molecular simulations, Comput. Phys. Commun. 181 (2010) 1477.
[27] S. Grimme, Supramolecular Binding Thermodynamics by Dispersion-Corrected Density Functional Theory, Chem. Eur. J. 18 (2012) 9955.
[28] F. Weigend, R. Ahlrichs, Balanced Basis Sets of Split Valence, Triple Zeta Valence and Quadruple Zeta Valence Quality for H to Rn: Design and Assessment of Accuracy, Phys. Chem. Chem. Phys. 7 (2005) 3297.
[29] A.D. Becke, Density-functional thermochemistry. V. Systematic optimization of exchange-correlation functionals, J. Chem. Phys. 107 (1997) 8554.
[30] B. J. Sundell, A. Lawrance, J., A. Sharber, Seth, Lin, S. , J. Harrigan, D. , Co2-philic crosslinked polyethylene glycol-based membranes for acid and sour gas separations., U.S Patent No. 11718805 (2021) 119081.
[31] N. Moitra, J.J. Moreau, X. Cattoën, M.W.C. Man, Convenient route to water-sensitive sol–gel precursors using click chemistry, Chem. Commun. 46 (2010) 8416.
[32] W. Guo, R. Pleixats, A. Shafir, T. Parella, Rhodium Nanoflowers Stabilized by a Nitrogen-Rich PEG-Tagged Substrate as Recyclable Catalyst for the Stereoselective Hydrosilylation of Internal Alkynes, Adv. Synth. Catal. 357 (2015) 89.
[33] R. d'Arcy, N. Tirelli, Mitsunobu Reaction: A Versatile Tool for PEG End Functionalization, Macromol. Rapid Commun. 36 (2015) 1829.

[34] C. Bannwarth, S. Ehlert, S. Grimme, GFN2-xTB—An Accurate and Broadly Parametrized Self-Consistent Tight-Binding Quantum Chemical Method with Multipole Electrostatics and Density-Dependent Dispersion Contributions, J. Chem. Theory Comput. 15 (2019) 1652.
[35] J.A. Loch, C. Borgmann, R.H. Crabtree, Synthesis of PEG–iridium conjugates and their use as hydrogenation catalysts in a water/substrate two-phase medium, J. Mol. Catal. A: Chem. 170 (2001) 75.
[36] B.J. Sundell, K.-s. Lee, A. Nebipasagil, A. Shaver, J.R. Cook, E.-S. Jang, B.D. Freeman, J.E. McGrath, Cross-Linking Disulfonated Poly(arylene ether sulfone) Telechelic Oligomers. 1. Synthesis, Characterization, and Membrane Preparation, Ind. Eng. Chem. Res. 53 (2014) 2583.
[37] H.C. Kolb, M.G. Finn, K.B. Sharpless, Click Chemistry: Diverse Chemical Function from a Few Good Reactions, Angew. Chem. Int. Ed. 40 (2001) 2004.
[38] Z. Liu, Y. Liu, W. Qiu, W.J. Koros, Molecularly Engineered 6FDA-Based Polyimide Membranes for Sour Natural Gas Separation, Angew. Chem. Int. Ed. 59 (2020) 14987.
[39] G.O. Yahaya, A. Hayek, A. Alsamah, Y.A. Shalabi, M.M. Ben Sultan, R.H. Alhajry, Copolyimide membranes with improved H2S/CH4 selectivity for high-pressure sour mixed-gas separation, Sep. Purif. Technol. 272 (2021) 118897.
[40] B. Kraftschik, W.J. Koros, Cross-Linkable Polyimide Membranes for Improved Plasticization Resistance and Permselectivity in Sour Gas Separations, Macromol. 46 (2013) 6908.
[41] S. Yi, B. Ghanem, Y. Liu, I. Pinnau, W.J. Koros, Ultraselective glassy polymer membranes with unprecedented performance for energy-efficient sour gas separation, Sci. Adv. 5 (2019) eaaw5459.
[42] Y. Liu, Z. Liu, G. Liu, W. Qiu, N. Bhuwania, D. Chinn, W.J. Koros, Surprising plasticization benefits in natural gas upgrading using polyimide membranes, J. Membr. Sci. 593 (2020) 117430.
[43] E. Favvas, F. Katsaros, S. Papageorgiou, A. Sapalidis, A. Mitropoulos, A review of the latest development of polyimide based membranes for CO 2 separations, React. Funct. Polym. 120 (2017) 104.
[44] M.A. Abdulhamid, G. Genduso, Y. Wang, X. Ma, I. Pinnau, Plasticization-Resistant Carboxyl-Functionalized 6FDA-Polyimide of Intrinsic Microporosity (PIM–PI) for Membrane-Based Gas Separation, Ind. Eng. Chem. Res. 59 (2020) 5247.
[45] G. Chatterjee, A.A. Houde, S.A. Stern, Poly(ether urethane) and poly(ether urethane urea) membranes with high H2S/CH4 selectivity, J. Membr. Sci. 135 (1997) 99.